Journal of Thermal Analysis and Calorimetry (2021) 146:1667–1678
https://doi.org/10.1007/s10973-020-10147-6

Non-isothermal cold crystallization kinetics of cork–polymer biocomposites based on polylactic acid for fused filament fabrication

S. P. Magalhães da Silva[1,2,3] · **Mónica A. Silva**[4] · **José M. Oliveira**[1,2,3]

Received: 12 March 2020 / Accepted: 31 July 2020 / Published online: 17 August 2020

Abstract
Cork–polymer composites (CPC) based on polylactic acid (PLA) matrix were prepared for the development of filaments for fused filament fabrication. The non-isothermal cold crystallization behaviours of PLA and CPC were investigated by differential scanning calorimetry. Cold crystallization kinetic behaviours of PLA and CPC with 15 mass/% of cork powder residues at different heating rates (1.25, 2.5, 5 and 7.5 K min^{-1}) were studied. Results showed that cold crystallization temperature (T_{cc}) of PLA matrix decreased with the addition of cork. Crystallization kinetic behaviour was studied by Avrami and Tobin models. It was shown that cork powder surface acts as a nucleating agent during non-isothermal cold crystallization, by accelerating the crystallization rate and, therefore, by reducing the half-time crystallization ($t_{1/2}$) values. Polarized optical microscopy and X-ray diffraction were used to evaluate the crystalline structure of PLA and CPC. Kissinger and Friedman methods were employed to determine the crystallization activation energy (E_c).

Keywords Cork · Biocomposites · Thermoplastics · Differential scanning calorimetry (DSC) · Crystallization kinetics

Introduction

Current concerns regarding the environment and increasing awareness about sustainability are pushing forward the development of new composite materials, which incorporate renewed materials. Cork is a reliable and sustainable raw material.

Cork is the outer bark of the cork oak tree *Quercus suber L.* and presents tiny hollow cells of hexagonal shape in closed-cell foam. Its main chemical composition is 33–50% of suberin, 20–25% of lignin, 12–20% of polysaccharides and 14–18% of extractives [1]. Portugal is the world's leading cork producer, and its main application is the production of stoppers. From stoppers production, a considerable amount of cork residues is generated (≈30 mass/%) [2]. The incorporation of these residues into polymeric matrices can be a suitable solution for the development of new materials solutions tailoring the needs of different applications.

Polylactic acid (PLA) is a biodegradable thermoplastic aliphatic polyester derived from renewable resources. It is a strong candidate to be used as a polymeric matrix due to its biodegradability and chemical compatibility. Different synthesis routes for PLA polymerization can be applied, and the most common one is the ring-opening lactide polymerization [3]. PLA stereochemical structure can be easily changed, depending on the amount of L- and D-isomers during polymerization [3]. This ratio of L- and D-isomers affects the mechanical and thermal properties of the obtained PLA. Regarding thermal properties, PLA can be a semi-crystalline or an amorphous material depending on its stereochemical structure and thermal history [4]. Moreover, PLA has a particular thermal behaviour in a way that multiphase transitions, such as glass transition, chain relaxation, cold crystallization and melting, are involved [5, 6]. The main drawback of PLA for commercial applications is its low crystallization rate. Several modifications have been

✉ S. P. Magalhães da Silva
sarapms@ua.pt

1 EMaRT Group – Emerging: Materials, Research, Technology, Aveiro, Portugal

2 School of Design, Management and Production Technologies, University of Aveiro, Estrada do Cercal, 449, Santiago de Riba-Ul, 3720-509 Oliveira de Azeméis, Portugal

3 Aveiro Institute of Materials (CICECO), University of Aveiro, Campus Universitário de Santiago, 3810-193 Aveiro, Portugal

4 Centro de Ciência e Tecnologia Têxtil (2C2T), University of Minho, Campus de Azurém, 4800-058 Guimarães, Portugal

proposed to improve the crystallization rate, mainly by the addition of nucleating agents [5, 7–11] or by the addition of plasticizers [12–14].

Additive manufacturing (AM) offers a set of techniques that opens a possibility of creating new products with a high level of design freedom. Fused filament fabrication (FFF), one of the AM techniques, is an extrusion-based process, in which a plastic filament is heated and selectively extruded via a nozzle layer by layer [15]. It is a disruptive technology on a constant growing market demanding for materials innovation. The combination of biodegradable polymer matrices with natural materials could be a sustainable solution for the development of new materials for AM. More specifically, considering the actual technological demand, cork–polymer composites (CPC) should be used to open new horizons in AM.

Cork–polymer composites (CPC) are a viable and a possible strategy for upgrading cork industrial residues based on sustainable development. The incorporation of lignocellulosic materials into polymeric matrices can bring several advantages. Some examples of these advantages are biodegradability, low density and hardness, low cost, easy availability, high levels of filling, good relation between strength and mass, good insulation/noise absorption properties and non-toxicity [16, 17]. Among other factors, CPC mechanical performance is influenced by the interaction of polymer and filler and by the crystallization behaviour of the matrix in the presence of the filler. Natural fibres and processing conditions can have an effect on polymer crystallization behaviour. Oliveira et al. [18, 19] showed that cork acted as a nucleating agent in a polypropylene (PP) matrix. To the better of our knowledge, few studies analysed the effect of cork on PLA crystallinity [20–23] and, so far, none of the studies are related to the crystallization kinetics. In this work, the physical/chemical changes in PLA during its melting, the non-isothermal cold crystallization kinetics of PLA and CPC and the nucleating ability of cork in a PLA matrix will be studied. The influence of cork on the nucleation and the crystal growth behaviour of PLA will be analysed by Avrami [24, 25] and Tobin [26–28] models. Crystallization activation energies (E_c) will be determined through Kissinger and Friedman methods [29, 30]. In addition, the morphology and crystalline structure of PLA and CPC were evaluated recurring to scanning electron microscopy (SEM), polarized optical microscopy (POM) and X-ray diffraction (XRD) techniques.

Experimental

Materials

Cork powder from a Portuguese cork producer was used. The material was fractionated through sieving (Retsch, Germany), and the fraction retained in the sieve of 20 µm was kept. Cork powder was dried in a vacuum oven (343 K) for 24 h. The average pore diameter, as well as the bulk density of cork powder, was measured by mercury intrusion porosimetry (MIP). The experiment was conducted in a Micromeritics AutoPore IV 9500 apparatus with pressure ranging from 0.3 to 227 MPa. The pore diameter was obtained by the Washburn equation [31], considering a surface tension of 0.485 N m^{-1} and a contact angle of 130° between cork and mercury.

The polymeric matrix used was an Ingeo™ Biopolymer PLA 4032D purchased from NatureWorks with a stereoisomer composition of 1.2–1.6% D-isomer lactide and a melting point between 428 and 443 K.

CPC compounding

Before compounding, the cork particles and the PLA were dried at 343 K for 24 h, in a vacuum oven (Carbolite AX60 model), to stabilize the moisture content. CPC formulation was made in a Brabender-type internal mixer. Initially, PLA pellets were charged and melted at 463 K, for 2 min at 40 rotations per minute (rpm), and then cork powder was added for additional 8 min. Previous studies reported that cork structure and composition do not alter at temperatures below 523 K [32, 33]. After compounding, the mixture was granulated in a Dynisco granulator into granules (0.5–1.0 mm). CPC formulation contains 85 mass/% of PLA and 15 mass/% of cork powder, in terms of volume of 45 volume/% and 55 volume/%, respectively [18, 34]. The selection of this mass ratio was to guarantee the highest amount of cork incorporated into PLA, in order to obtain a CPC filament with a non-plastic and natural touch, similar to cork.

Characterization by SEM

SEM Hitachi SU-70 equipment was used to morphologically analyse cork powder particles and cork dispersion into PLA matrix after compounding. Samples were mounted on aluminium stubs and sputter-coated (Polaron E5000) with Au/Pd target for 2 min at 12 mA.

Characterization by DSC

Thermal properties and non-isothermal crystallization behaviour of PLA and CPC were studied using Shimadzu DSC-60 equipment. All experiments were carried out in nitrogen atmosphere (50 mL min^{-1}). Samples between 9.0 and 10.0 mg were hermetically sealed in aluminium pans. Each sample was heated from 293 to 473 K at a scan rate of 20 K min^{-1} and held for 5 min at this temperature to eliminate the thermal history. Then, the samples were cooled at 20 K min^{-1} to room temperature (≈293 K) and heated again

up to 473 K. Four different heating rates were used, namely 1.25, 2.5, 5 and 7.5 K min^{-1}. The selection of the cooling rates was based on the low kinetics of PLA. A study of Miyata and Masuko [35] showed that samples cooled at rates higher than 10 K min^{-1} did not crystallize and remained amorphous. Only the second run was considered for analysis. Glass transition temperature (T_g), cold crystallization temperature (T_{cc}), melting temperature (T_m), cold crystallization enthalpy (ΔH_{cc}) and melting crystallization enthalpy (ΔH_m) of PLA and CPC were determined from the DSC thermographs. The crystallinity degree (X_c) of samples was calculated using Eq. (1):

$$X_c = \frac{\Delta H_{cc}}{\Delta H_m^0 (1 - m)} \times 100, \tag{1}$$

where m is the mass percentage of the filler and ΔH_m^0 is the melting crystallization enthalpy for 100% crystalline PLA (93 J g^{-1}) [36].

Characterization by POM

POM was performed to evaluate the nucleation and spherulites growth in pure PLA and in PLA in the presence of cork powder. The observations were made on a Nikon Eclipse L150. Firstly, both samples were melted at 463 K for 5 min to remove thermal history. Then, the samples were cooled down to 393 K. Isothermal crystallization took place at 393 K for 15 min.

Characterization by XRD

Panalytical X'Pert Pro 3 equipment with a Cu Kα ($\lambda = 1.5406$ Å) radiation source was used. Diffraction intensities were measured from 10º to 40º with a step size of 0.02. XRD measurements were performed at 298 K.

Theoretical principles

Non-isothermal kinetic parameters were determined by Avrami [24, 25], Tobin [26–28], Kissinger [29] and Friedman [30] models. The relative degree of crystallinity at time t (X_t), as a function of temperature (T), was determined through Eq. (2):

$$X_t = \frac{\int_{T_0}^{T} \left(\frac{dH_{cc}}{dT}\right) dT}{\int_{T_0}^{T_\infty} \left(\frac{dH_{cc}}{dT}\right) dT}, \tag{2}$$

where T_0 and T_∞ are the temperatures corresponding to the onset and end of the crystallization process, respectively.

In the case of the non-isothermal cold crystallization process, the relationship between the crystallization time (t) and the corresponding temperature (T) can be obtained by Eq. (3):

$$t = \frac{|T_0 - T|}{\varphi}, \tag{3}$$

where ϕ is the heating rate.

Avrami model [24, 25] is commonly used to describe the isothermal crystallization kinetic behaviour and analyse the increase in relative crystallinity with time:

$$1 - X_t = \exp\left(-Z_t t^n\right), \tag{4}$$

where Z_t is the crystallization rate constant, containing the nucleation and growth rate parameters, and it is temperature dependent, and n is the Avrami index which is dependent on the nucleation type and on the growth geometry of the crystals. The linearized form can be written as follows:

$$\log\left[-\ln\left(1 - X_t\right)\right] = \log\left(Z_t\right) - n\log(t) \tag{5}$$

Mandelkern [37] considered that the primary non-isothermal crystallization stage can be described through Avrami model, based on a constant crystallization temperature assumption. The n and Z_t parameters do not have the same physical meaning as in the isothermal crystallization processes, since the temperature changes constantly during non-isothermal crystallization. Jeziorny [38] calibrated the Z_t parameter, considering the temperature dependence of the non-isothermal crystallization, correcting the crystallization rate constants by introducing heating rate:

$$\log Z_c = \frac{\log(Z_t)}{\varphi} \tag{6}$$

The time required to achieve 50% of crystallization is called half-time of crystallization ($t_{1/2}$), and it is considered as a prime parameter for investigating the kinetics of crystallization process. The $t_{1/2}$ for non-isothermal crystallization can be obtained from the following expression [39]:

$$t_{1/2} = \left(\frac{\ln 2}{Z_t}\right)^{1/n} \tag{7}$$

Tobin [26–28] model was utilized to study the phase transformation kinetics with growth site impingement on the non-isothermal crystallization kinetics of PLA and CPC (Eq. 8):

$$X_t = \frac{K_T t^{n_T}}{1 + K_T t^{n_T}}, \tag{8}$$

where K_T and n_T correspond to Tobin crystallization rate constant and Tobin exponent, respectively. The n_T parameter provides information about the type of nucleation and growth mechanism involved in the non-isothermal crystallization process. The linearized form of Eq. (9) is rewritten as follows:

$$\ln\left(\frac{X_t}{1-X_t}\right) = \ln K_T + n_T \ln t \tag{9}$$

Kissinger [29] method was applied to determine E_c for non-isothermal cold crystallization of neat PLA and CPC. E_c is the energy required for the movement of PLA molecular segments from melt to the crystal growth surface. It is determined by the variation in T_{cc} with respect to φ, as described in Eq. (10):

$$\frac{-E_C}{R} = \frac{d\left(\ln\left(\frac{\varphi}{T_{cc}^2}\right)\right)}{d\left(\frac{1}{T_{cc}}\right)}, \tag{10}$$

where R is the gas constant and T_{cc} is the cold crystallization temperature.

An isoconversional method developed by Friedman [30] was also used to determine E_c. Contrarily to the Kissinger method, where a single value of E_c is determined, regardless of the kinetics of the system, from the Friedman method it is evaluated the dependency of E_c with crystallinity and temperature. According to Friedman, different effective activation energies can be calculated for each X_t considering Eq. 11:

$$\ln\left(\frac{dX}{dt}\right)_{X,i} = \text{contant} - \frac{E_c}{RT_{X,i}}, \tag{11}$$

where i represents each heating rate applied, (dX/dt) is the instantaneous crystallization rate as a function of time at a given conversion X and $T_{X,i}$ is the temperature associated with a given conversion X at different i's. At a given X_t, E_c can be calculated from the slope (E_c/R) of the correlation between $\ln(dX/dt)$ versus $1/T_X$.

Results and discussion

Cork powder characterization

MIP analysis was applied to characterize cork powder in terms of density and porosity. Table 1 shows the average value of pore diameter, the porosity and bulk and apparent densities.

According to IUPAC [40], cork powder pores are classified as macropores, since they present an average diameter greater than 50 nm. Cork powder presents low density and high porosity, which is mainly due to its characteristic honeycomb structure, as shown in Fig. 1.

Non-isothermal heating behaviour

Non-isothermal DSC curves of neat PLA and CPC from the second heating scan at different heating rates are represented in Fig. 2. Exothermic cold crystallization peaks appear for both, pure PLA and CPC. The PLA molecular chains become mobile above T_g, allowing crystallization. Above T_g, molecular chains possess the ability to be partly ordered and the cold crystallization takes place. These crystals melt upon further heating. For PLA, cold crystallization peaks become smoother as the heating rate increases. It suggests that lower scan rates during heating can promote PLA crystallization [6]. In Fig. 2, the T_m peaks for PLA and CPC are also visible.

There are double melting peaks for both samples, which are usually ascribed to simultaneous occurrence of thinner lamellae melting and recrystallization. More specifically, the lower T_m peak is usually associated with the melting of some original crystals grown by primary crystallization, while the higher T_m peak is associated with the melting of crystals formed through a melt–recrystallization process during the heating process in DSC measurement [7, 41]. Other studies, involving biomaterials, allowed us to visualize the presence of double T_m peaks in the crystallization behaviour of PLA [20, 42]. The presence and reorganization of different types of crystals with different stabilities were the explanation given by the authors to the appearance of these double melting peaks. As the heating rate increases, these double melting peaks became weak for both samples. The same tendency was reported by Zhang and co-workers [41]. They appointed a decrease in the rate of crystallization based on the self-adjustment of the amorphous PLA chains. The non-isothermal crystallization parameters obtained from Fig. 2 and equations are listed in Table 2.

The T_g values for PLA and CPC slightly increase with heating rate, which can suggest the confinement of the amorphous mobile phase [20]. In fact, for each material, the T_{cc} values also increase with heating rate, supporting the reduced ability of PLA to recrystallize on heating above T_g. In addition, as T_{cc} shifts to higher values with heating rate, it implies that the crystallization process occurs earlier for lower heating rates [41]. At a given heating rate, the values

Table 1 Cork powder characterization

Cork powder	
Average pore diameter/μm	16.9
Bulk density/g cm^{-3}	0.177
Apparent density/g cm^{-3}	0.616
Porosity/%	71.3

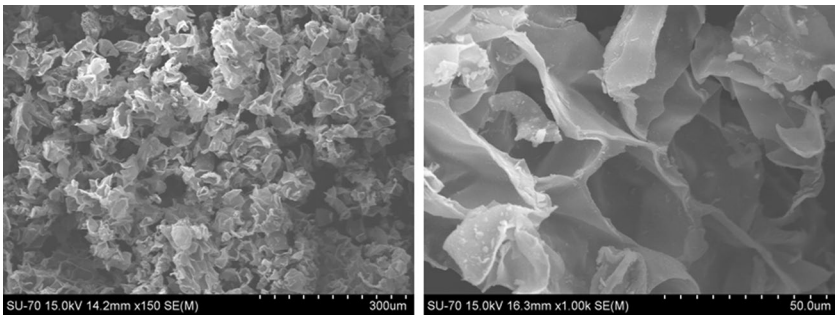

Fig. 1 SEM images of cork powder

for T_{cc} of CPC were lower than for neat PLA. This indicates that cork can promote the initial cold crystallization of the PLA matrix due to the heterogeneous nucleation effect. Values of ΔH_{cc} present a downward trend as the heating rate increases. Considering that all samples were initially amorphous, as a consequence of the fast cooling rate applied, this trend indicates that, as the heating increases, polymer chains did not have sufficient time to form crystalline structures. In parallel, ΔH_m values exhibit the same trend as ΔH_{cc}. This can be an indication that PLA melting behaviour depends on the crystal structures created during cold crystallization phase. A study of Nofar et al. [5] reported the same behaviour. From the X_{cc} values, it is noticed that the amount of crystallinity developed in PLA is dependent on the heating rate. X_{cc} values increased with the addition of cork, indicating that cork facilitated the crystallization of PLA during heating.

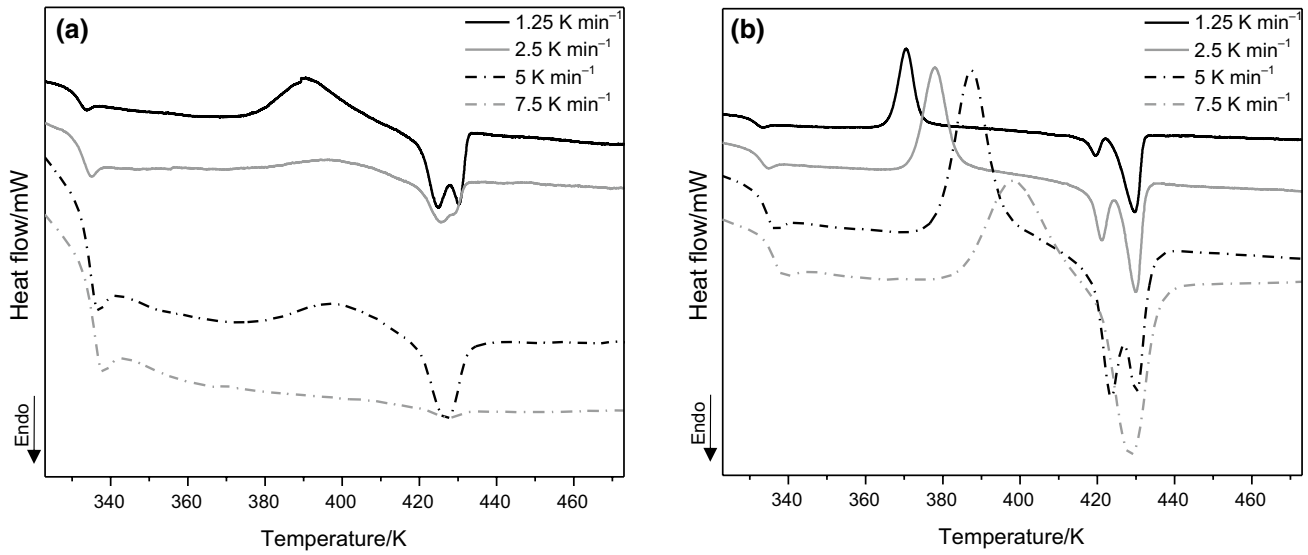

Fig. 2 DSC thermographs, in the second heating cycle, at different heating rates for **a** PLA and **b** CPC

Table 2 Non-isothermal crystallization parameters of PLA and CPC materials

Sample	ϕ/K min^{-1}	T_g/K	T_{cc}/K	ΔH_{cc}/J g^{-1}	X_{cc} /%	T_m/K	ΔH_m/J g^{-1}
PLA	1.25	335.2	389.6	13.6	14.7	424.4/430.7	11.3
	2.50	335.0	398.5	4.8	5.2	425.9/428.2[a]	3.9
	5.00	337.8	401.5	1.3	1.4	426.4	2.6
	7.50	337.7	405.7	0.2	0.3	426.9	0.2
CPC	1.25	334.6	370.5	21.8	27.5	419.8/429.9	15.8
	2.50	335.3	378.0	16.8	21.2	421.6/430.0	15.0
	5.00	337.4	387.8	16.4	20.7	423.9/429.8	15.7
	7.50	339.4	398.5	11.6	14.6	429.2	12.8

[a]Shoulder

Cork may act as a heterogeneous nucleating agent. The ability of cork to modify the crystallization behaviour of PLA may be associated with the increased density of nucleating sites provided by cork particles. This nucleating ability of cork was also observed in other studies considering bio-based polyesters acting as matrices [20, 22, 43]. Figure 3 represents the non-isothermal DSC curves of neat PLA and CPC at 1.25 K min^{-1}.

As referred above, the presence of cork shifted T_{cc} to lower values, showing the nucleating ability of cork. Its addition also led to a more well-defined and sharp cold crystallization peak, which usually corresponds to a well-defined crystal structure. This suggests that, somehow, the addition of cork resulted in a rearrangement of PLA molecules leading to a more defined crystal structure.

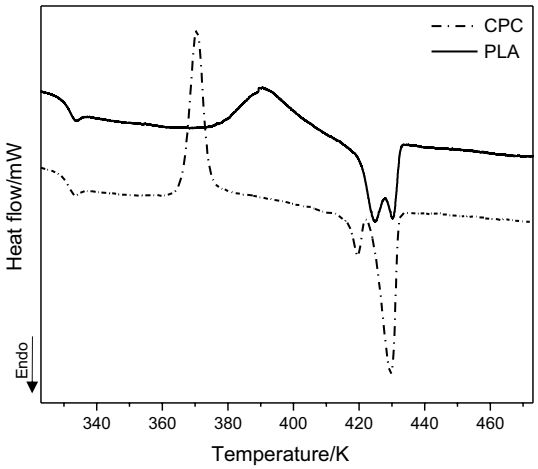

Fig. 3 DSC thermographs of PLA and CPC, at a heating rate of 1.25 K min^{-1}

Non-isothermal cold crystallization kinetics

The relative crystallinity curves versus crystallization time for the PLA and CPC studied samples are shown in Fig. 4. At different heating rates, curves exhibit the same sigmoidal shape. The first nonlinear part is usually considered the nucleation step of the crystallization process [44]. The longest nucleation step occurs for PLA at 1.25 K min^{-1}, resulting in the formation of more nuclei. The curvature of the second nonlinear part levelled off that is attributed to the impingement or crowding of spherulites at the later stage of the crystal growth [45].

Higher heating rates have managed to complete the PLA crystallization process in a shorter time. This behaviour is also observed through $t_{1/2}$ parameter (Table 3). A shorter $t_{1/2}$ value means a faster crystallization process, where a shorter time is needed to achieve 50% of crystallization fraction. It is visible a decrease in $t_{1/2}$ for all heating rates when PLA crystallizes in the presence of cork when compared to neat PLA. Once again, the nucleating effect of cork is observed. The higher $t_{1/2}$ values observed for PLA and CPC at lower heating rates can be attributed to the secondary crystallization process.

Avrami model

Avrami plots and kinetic parameters are shown in Fig. 5 and Table 3, respectively, obtained from the application of Eqs. (5) and (6). It was considered that X_t values range from 10 to 80%.

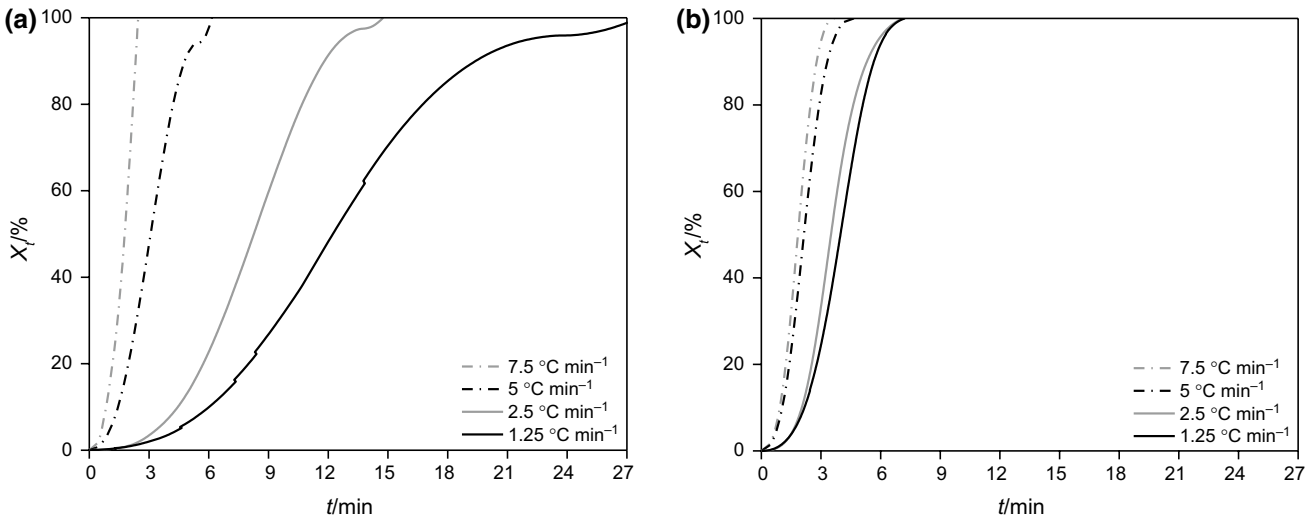

Fig. 4 Relative crystallinity (X_t) versus time (t) for **a** PLA and **b** CPC

Avrami model was adequate to describe the non-isothermal cold crystallization kinetics of neat PLA and CPC. (R^2 is equal to 1 for almost all heating scan rates.) It should be noted that Avrami model does not have the same physical meaning as in the isothermal crystallization, owing to the constant variation of temperature in non-isothermal crystallization.

This temperature dependence will have an effect on the rates of both nuclei formation and spherulite growth. Z_c values increased with heating rate, demonstrating that cold crystallization rate increases with heating rate. The n values for PLA and CPC are found in the range of ~ 2–3. Non-integer n values reveal a combination of thermal and athermal nucleation mechanisms [7]. The average n values for PLA and CPC were 2.78 and 3.02, respectively, indicating that the non-isothermal cold crystallization was initiated by an athermal nucleation and followed by a mixed two- and three-dimensional spherulite growth [7, 14].

Table 3 Half-time crystallization and Avrami kinetic parameters

Sample	ϕ/K min^{-1}	$t_{1/2}$/min	n	Z_c/min^{-n} K^{-1}	R^2
PLA	1.25	12.2	2.7	3.46E−03	0.999
	2.50	8.20	3.1	6.28E−02	0.999
	5.00	3.10	2.5	5.26E−01	0.999
	7.50	1.70	2.8	7.75E−01	0.989
CPC	1.25	3.90	3.2	2.20E−02	0.999
	2.50	3.60	3.4	1.58E−01	0.999
	5.00	2.10	2.7	6.16E−01	0.999
	7.50	1.80	2.8	7.59E−01	0.999

Tobin model

Tobin model was considered to overcome the limitation of Avrami model in the study of the early stage of crystallization process. More specifically, Tobin model is able to describe the phase transformation kinetics with growth site impingement as well as secondary crystallization process [26–28]. Contrarily to Avrami exponent, Tobin exponent n_T does not need to be integer, since it is controlled directly by different types of nucleation and growth mechanisms [10].

Tobin plots for PLA and CPC obtained at different heating rates are shown in Fig. 6, and the related parameters are presented in Table 4. An X_t range of 10–80% was used for calculations.

The n_T average value of PLA is 3.60 and CPC is 3.93. For both cases, n_T values are almost independent of the heating rate.

Concerning the K_T parameter, it increases as the heating rate increases. The K_T values for CPC are larger than for PLA, which indicates that the presence of cork accelerates the non-isothermal cold crystallization of PLA. Tobin parameters describe the same physical significance analogous to that of Avrami model. In this study, Tobin parameters exhibited a similar tendency to those obtained for Avrami analysis.

Comparison between Avrami and Tobin models

The efficiency of both models on describing the non-isothermal crystallization kinetics of PLA and CPC can be assessed from Fig. 7. For each heating rate, the curve that correlates X_t versus t (as in Fig. 4) was used as a reference.

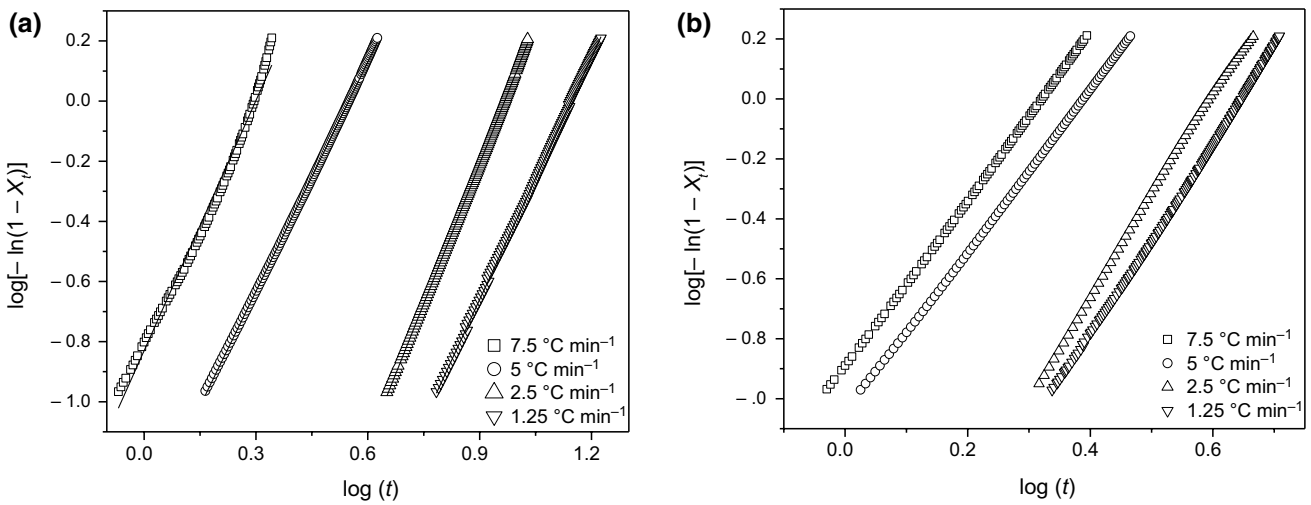

Fig. 5 Avrami plots of **a** PLA and **b** CPC

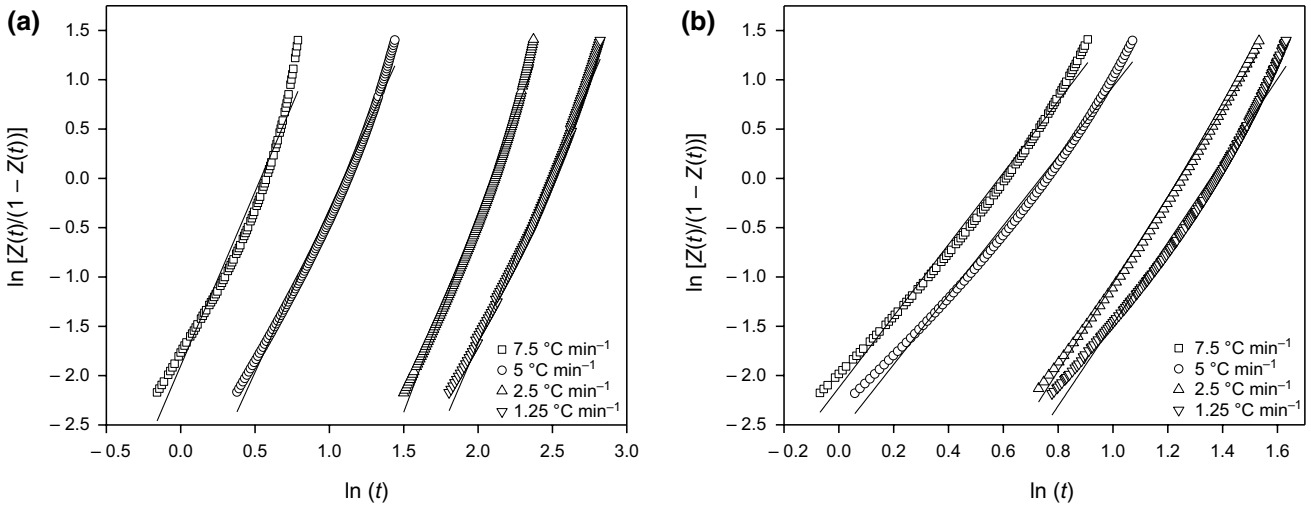

Fig. 6 Tobin plots of **a** PLA and **b** CPC

Table 4 Tobin kinetic parameters

Sample	ϕ/K min^{-1}	n_T	K_T/min^{-n}	R^2
PLA	1.25	3.5	1.7E−04	0.99
	2.5	4.0	2.2E−04	0.99
	5	3.3	2.7E−02	0.99
	7.5	3.5	1.5E−01	0.97
CPC	1.25	4.1	3.6E−03	0.99
	2.5	4.4	4.1E−03	0.99
	5	3.5	7.5E−02	0.99
	7.5	3.6	1.2E−01	0.99

Considering the kinetic parameters displayed in Tables 3 and 4, as well as Eqs. (4) and (8), the fitting accuracy of Avrami and Tobin models was determined.

According to Fig. 7, a similar tendency was observed for PLA and CPC samples. The accuracy of Avrami model fitting becomes higher as the heating rates increase. On the contrary, for each heating rate, Tobin model fitting underpredicts the evolution of relative crystallinity. This tendency is more accentuated at higher relative crystallinity values ($X_t \geq 75\%$). Working with syndiotactic polypropylene, Supaphol [46] observed a deviation of the Tobin model fitting, which was attributed to the use of a simplified form of Eq. (8) or it could be associated with the overprediction of the impingement effect.

Activation energy

Kissinger plots are shown in Fig. 8, and the corresponding E_c values are listed in Table 5. The plots exhibit good linearity, and regression coefficients (R^2) values are obtained with the values of ~ 0.990.

The addition of cork resulted in a decrease in the E_c, from 141.5 to 63.3 kJ mol^{-1}, suggesting that the energy barrier of cold crystallization is lower for CPC, causing an increase in crystallization ability for CPC as compared with PLA, an expected result since cork acted as a nucleating agent, as presented before. Comparable results have also been found for the cold crystallization activation energy of PLA in the presence of multiwalled carbon nanotubes [47], clay [6] and a combination of several nucleating agents [48].

The dependency of E_c as a function of X_t was evaluated according to the Friedman method. X_t values ranging from 0.1 to 0.8 were considered, and the value of R^2 was obtained from 0.95 to 0.99. Figure 9 shows E_c versus X_t for both materials, and the corresponding average E_c values are listed in Table 6.

The E_c values indicate that the energy barrier for the cold crystallization process is lower for the composite than for the unfilled PLA. The same tendency was observed in similar studies [49, 50]. The results are also in agreement with those obtained in the previous kinetic analysis, reinforcing the nucleating ability of cork. In fact, for X_t equal to 0.1, the E_c values acquired from Kissinger method are similar to E_c values from Friedman method. This can be indicative that the Kissinger method can represent one E_c value obtained by Friedman, as also observed by Li et al. [7] and Ries et al. [50].

Morphology and POM observations

The morphology of CPC was evaluated by SEM, and it is represented in Fig. 10.

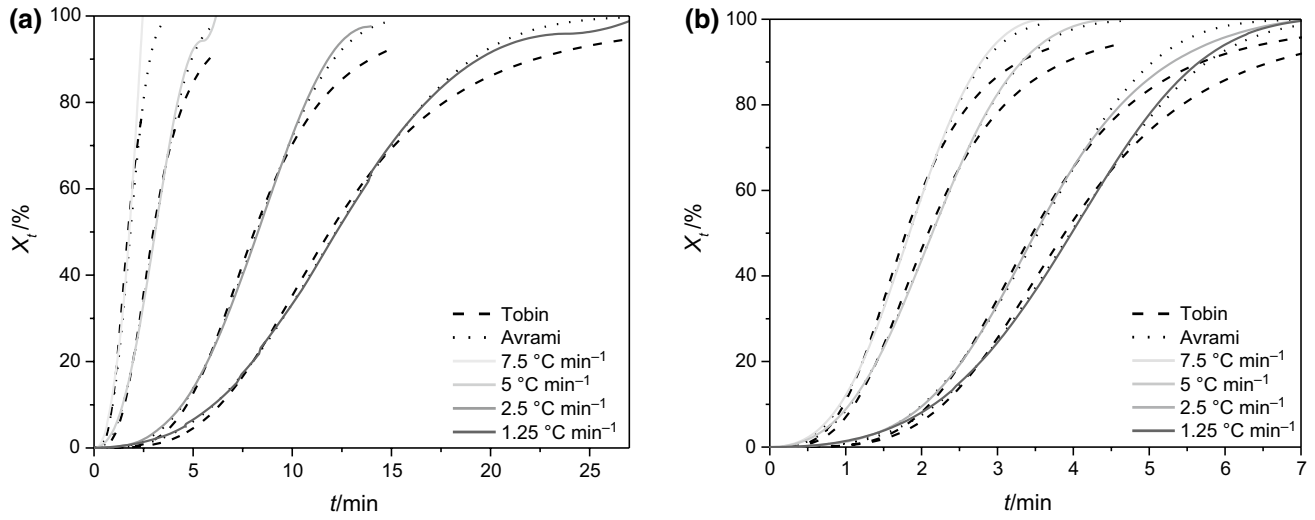

Fig. 7 Comparison between Avrami and Tobin models—relative crystallinity (X_t) as a function of time (t) for **a** PLA and **b** CPC

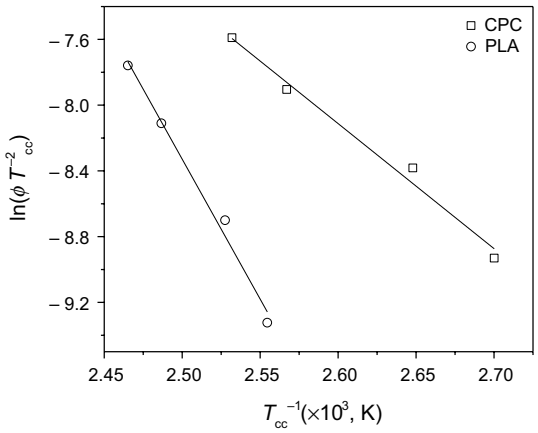

Fig. 8 Kissinger plots for PLA and CPC

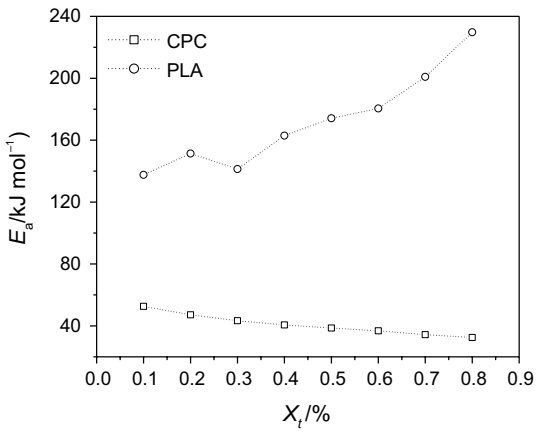

Fig. 9 Dependency of E_c as a function of X_t for PLA and CPC

Table 5 Activation energies for PLA and CPC according to Kissinger method

Sample	E_c/kJ mol^{-1}	R^2
PLA	141.5	0.990
CPC	63.3	0.986

Table 6 Average activation energies ($\bar{E}_c$) for PLA and CPC according to Friedman method

Sample	$\bar{E}_c$/kJ mol^{-1}
PLA	172.3
CPC	40.8

It is seen that cork particles are homogeneously dispersed and imbibed within PLA matrix. Cork particles are completely covered by PLA (highlighted in orange).

The evaluation of cork powder as a nucleating agent in PLA matrix was performed through POM. Optical micrographs of pure PLA and CPC after 15 min at 393.2 K are shown in Fig. 11.

It is revealed the nucleating ability of cork powder in PLA matrix, already determined by the non-isothermal crystallization kinetic analyses. Within 15 min, CPC exhibited higher nucleation density and smaller spherulite size when compared to pure PLA. The same tendency was visualized by Li et al. [51].

XRD

XRD analyses were performed to evaluate PLA and CPC crystalline structures. PLA exhibits several polymorphisms during melt or cold crystallization, such as α-, β- and γ-forms [52, 53]. The α-form is considered the most stable, and it is produced at high crystallization temperatures (> 393.2 K), while a disordered α′-form can be developed

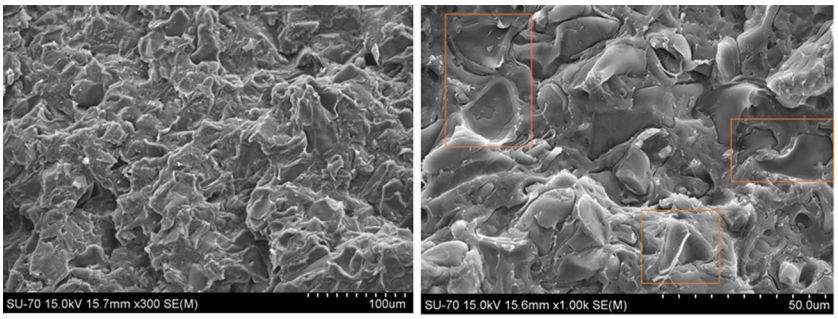

Fig. 10 SEM images of CPC after compounding

at lower temperatures [52, 54, 55]. A combination of these α forms is usually made in industrial processes to decrease PLA processing temperature. Figure 12 displays the XRD patterns of PLA and CPC measured at 298.2 K.

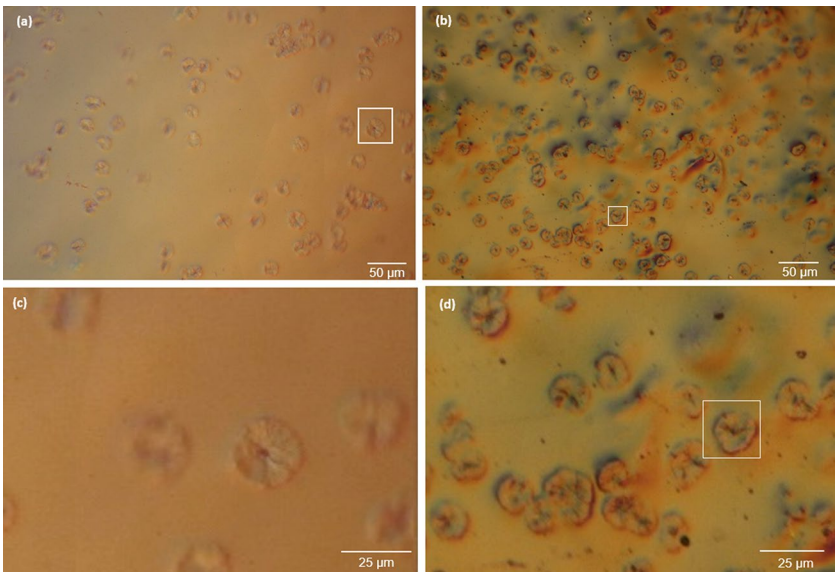

Fig. 11 Optical micrographs of **a–c** PLA and **b–d** CPC (15 min at 393.2 K)

For PLA, two characteristic reflection planes of α-phase crystals can be identified, namely (200)/(110) and (203), with scattering angles (2θ) of 16.9° and 19.2°, respectively [52, 54]. As for CPC, stronger peaks at 16.9° and 19.2° can be observed, indicating that cork can improve the crystallization of PLA. In addition, the presence of cork during the cold crystallization of PLA alters its crystalline structure, which is reflected by the appearance of α-phase characteristic peaks, namely at 11.9° (110), 22.6° (015) and 27.4° (207) [52, 54, 56]. These findings are in agreement with those obtained by the non-isothermal crystallization kinetic analyses.

Conclusions

The non-isothermal cold crystallization behaviours of PLA and CPC were investigated at different heating rates (1.25, 2.5, 5 and 7.5 K min^{-1}) through DSC measurements. In the presence of cork, T_{cc} shifted to lower values, revealing that cork facilitates the initial cold crystallization of the PLA matrix. Additionally, an increase of ~ 300% of X_{cc} was observed when PLA cold crystallizes in the presence of cork. Avrami and Tobin models were applied to analyse the non-isothermal kinetics of the samples. Both methods successfully described the non-isothermal cold crystallization processes of PLA and CPC. The same tendency was attained for both methods, where the addition of cork increased the crystallization rate of PLA matrix and n values indicated a mixed two- and three-dimensional crystallization growth. These results were supported by POM and XRD analyses. From the Kissinger and Friedman methods, lower ΔE_C values for CPC were obtained, indicating a reduction in energy barrier for crystallization compared to neat PLA.

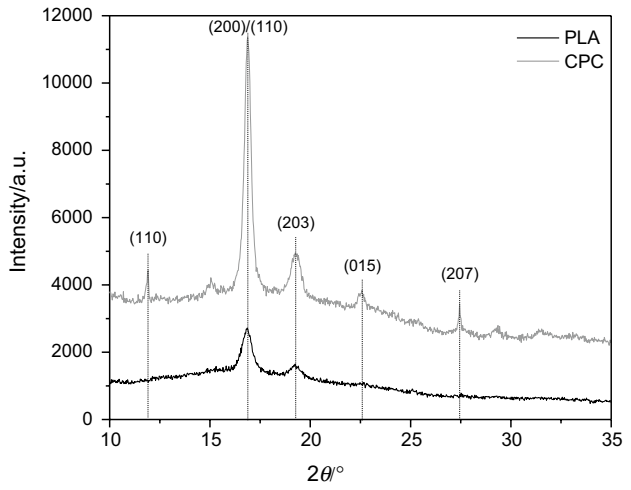

Fig. 12 XRD patterns of PLA and CPC

This study allows us to understand the cold crystallization behaviour of CPC filament during FFF, which is considered a fast local cooling process. As reported above, the addition of cork to PLA considerably increased the crystallization rate and X_{cc}, revealing the ability of PLA to crystallize rapidly in the presence of cork, as experienced during FFF. This will have an impact on the mechanical behaviour of printing parts. The presence of small spherulites will enhance ductility and impact strength. It will also help in defining printing settings and in evaluating layers adhesion and warpage.

Acknowledgements This work was supported by COMPETE 2020 – Programa Operacional Competividade e Internacionalização within TT@ESAN project (NORTE-01-0246-FEDER-000001). The authors would like to acknowledge Maria Celeste Coimbra Azevedo for the DSC measurements and Artur Sarabando for the XRD analyses.

References

1. Pereira H. Cork: biology, production and uses. Amsterdam: Elsevier; 2007.
2. Fernandes EM, Aroso IM, Mano JF, Covas JA, Reis RL. Functionalized cork-polymer composites (CPC) by reactive extrusion using suberin and lignin from cork as coupling agents. Compos Part B Eng. 2014;67:371–80.
3. Garlotta D. A literature review of poly(lactic acid). J Polym Environ. 2001;9:63–84.
4. Magoń A, Pyda M. Study of crystalline and amorphous phases of biodegradable poly(lactic acid) by advanced thermal analysis. Polymer (Guildf). 2009;50:3967–73.
5. Nofar M, Zhu W, Park CB, Randall J. Crystallization kinetics of linear and long-chain-branched polylactide. Ind Eng Chem Res. 2011;50:13789–98.
6. As'habi L, Jafari SH, Khonakdar HA, Häussler L, Wagenknecht U, Heinrich G. Non-isothermal crystallization behavior of PLA/LLDPE/nanoclay hybrid: synergistic role of LLDPE and clay. Thermochim Acta. 2013;565:102–13.
7. Li C, Dou Q. Non-isothermal crystallization kinetics and spherulitic morphology of nucleated poly(lactic acid): effect of dilithium cis-4-cyclohexene-1,2-dicarboxylate as a novel and efficient nucleating agent. Polym Adv Technol. 2015;26:376–84.
8. Ke T, Sun X. Melting behavior and crystallization kinetics of starch and poly(lactic acid) composites. J Appl Polym Sci. 2003;89:1203–10.
9. Qiu Z, Li Z. Effect of orotic acid on the crystallization kinetics and morphology of biodegradable poly(L-lactide) as an efficient nucleating agent. Ind Eng Chem Res. 2011;50:12299–303.
10. Han Q, Wang Y, Shao C, Zheng G, Li Q, Shen C. Nonisothermal crystallization kinetics of biodegradable poly(lactic acid)/zinc phenylphosphonate composites. J Compos Mater. 2014;48:2737–46.
11. Koutsomitopoulou AF, Bénézet JC, Bergeret A, Papanicolaou GC. Preparation and characterization of olive pit powder as a filler to PLA-matrix bio-composites. Powder Technol. 2014;255:10–6.
12. Li M, Hu D, Wang Y, Shen C. Nonisothermal crystallization kinetics of poly(lactic acid) formulations comprising talc with poly(ethylene glycol). Polym Eng Sci. 2010;50:2298–305.
13. Kulinski Z, Piorkowska E. Crystallization, structure and properties of plasticized poly(l-lactide). Polymer (Guildf). 2005;46:10290–300.
14. Xiao H, Yang L, Ren X, Jiang T, Yeh JT. Kinetics and crystal structure of poly(lactic acid) crystallized nonisothermally: effect of plasticizer and nucleating agent. Polym Compos. 2010;31:2057–68.
15. Gibson I, Rosen DSB. Additive manufacturing technologies: 3D printing, rapid prototyping, and direct digital manufacturing. 2nd ed. New York: Springer; 2015.
16. Fernandes EM, Correlo VM, Mano JF, Reis RL. Polypropylene-based cork–polymer composites: processing parameters and properties. Compos Part B Eng. 2014;66:210–23.
17. Thakur VK, editor. Lignocellulosic polymer composites: processing, characterization and properties. Hoboken: Scrivener Publishing, Wiley; 2015.
18. Magalhães da Silva SP, Lima PS, Oliveira JM. Non-isothermal crystallization kinetics of cork-polymer composites for injection molding. J Appl Polym Sci. 2016;133:44124–33.
19. Magalhães Da Silva SP, Lima PS, Oliveira JM. Nucleating ability of cork in polypropylene-based composites. In: ECCM 2016 - Proceeding 17th Eur Conf Compos Mater; 2016.
20. Fernandes EM, Correlo VM, Mano JF, Reis RL. Cork–polymer biocomposites: mechanical, structural and thermal properties. Mater Des. 2015;82:282–9.
21. Vilela C, Sousa AF, Freire CSR, Silvestre AJD, Pascoal Neto C. Novel sustainable composites prepared from cork residues and biopolymers. Biomass Bioenergy. 2013;55:148–55.
22. Daver F, Lee KPM, Brandt M, Shanks R. Cork–PLA composite filaments for fused deposition modelling. Compos Sci Technol. 2018;168:230–7.
23. Andrzejewski J, Szostak M, Barczewski M, Łuczak P. Cork-wood hybrid filler system for polypropylene and poly(lactic acid) based injection molded composites. Structure evaluation and mechanical performance. Compos Part B Eng. 2019;163:655–68.
24. Avrami M. Kinetics of phase change. II Transformation-time relations for random distribution of nuclei. J Chem Phys. 1940;8:212.
25. Avrami M. Kinetics of phase change. I General theory. J Chem Phys. 1939;7:1103.
26. Tobin MC. Theory of phase transition kinetics with growth site impingement. I. Homogeneous nucleation. J Polym Sci Polym Phys Ed. 1974;12:399–406.
27. Tobin MC. The theory of phase transition kinetics with growth site impingement. II. Heterogeneous nucleation. J Polym Sci Polym Phys Ed. 1976;14:2253–7.

28. Tobin MC. Theory of phase transition kinetics with growth site impingement. III. Mixed heterogeneous–homogeneous nucleation and nonintegral exponents of the time. J Polym Sci Polym Phys Ed. 1977;15:2269–70.
29. Kissinger HE. Variation of peak temperature with heating rate in differential thermal analysis. J Res Natl Bur Stand. 1934;1956(57):217–21.
30. Friedman HL. Kinetics of thermal degradation of char-forming plastics from thermogravimetry. Application to a phenolic plastic. J Polym Sci Part C Polym Symp. 1964;6:183–95.
31. Washburn EW. The dynamics of capillary flow. Phys Rev. 1921;17:273–83.
32. Şen A, Van den Bulcke J, Defoirdt N, Van Acker J, Pereira H. Thermal behaviour of cork and cork components. Thermochim Acta. 2014;582:94–100.
33. Rosa ME, Fortes MA. Thermogravimetric analysis of cork. J Mater Sci Lett. 1988;7:1064–5.
34. Magalhães da Silva SP, Lima PS, Oliveira JM. Rheological behaviour of cork-polymer composites for injection moulding. Compos Part B Eng. 2016;90:172–8.
35. Miyata T, Masuko T. Crystallization behaviour of poly(l-lactide). Polymer (Guildf). 1998;39:5515–21.
36. Fischer EW, Sterzel HJ, Wegner G. Investigation of the structure of solution grown crystals of lactide copolymers by means of chemical reactions. Kolloid Z Z Polym. 1973;251:980–90.
37. Mandelkern L. Methods of experimental physics. New York: Academic Press; 1980.
38. Jeziorny A. Parameters characterizing the kinetics of the non-isothermal crystallization of poly(ethylene terephthalate) determined by DSC. Polymer (Guildf). 1978;19:1142–4.
39. Liu Y, Wang L, He Y, Fan Z, Li S. Non-isothermal crystallization kinetics of poly(L-lactide). Polym Int. 2010;59:1616–21.
40. International Union of Pure, and Applied Chemistry (IUPAC). Recommendations for the characterization of porous solids (Technical Report). Pure Appl Chem. 1994;66:1739–58.
41. Wu D, Wu L, Wu L, Xu B, Zhang Y, Zhang M. Nonisothermal cold crystallization behavior and kinetics of polylactide/clay nanocomposites. J Polym Sci Part B Polym Phys. 2007;45:1100–13.
42. Masirek R, Kulinski Z, Chionna D, Piorkowska E, Pracella M. Composites of poly(L-lactide) with hemp fibers: morphology and thermal and mechanical properties. J Appl Polym Sci. 2007;105:255–68.
43. Magalhães da Silva SP, Antunes T, Costa MEV, Oliveira JM. Cork-like filaments for additive manufacturing. Addit Manuf. 2020;34:101229.
44. Ding W, Chu RKM, Mark LH, Park CB, Sain M. Non-isothermal crystallization behaviors of poly(lactic acid)/cellulose nanofiber composites in the presence of CO_2. Eur Polym J. 2015;71:231–47.
45. Abdel Aziz MS, Saad GR, Naguib HF. Non-isothermal crystallization kinetics of poly(3-hydroxybutyrate) in copoly(ester-urethane) nanocomposites based on poly(3-hydroxybutyrate) and cloisite 30B. Thermochim Acta. 2015;605:52–62.
46. Supaphol P. Nonisothermal bulk crystallization and subsequent melting behavior of syndiotactic polypropylenes: crystallization from the melt state. J Appl Polym Sci. 2000;78:338–54.
47. Zhao Y, Qiu Z, Yan S, Yang W. Crystallization behavior of biodegradable poly(L-lactide)/multiwalled carbon nanotubes nanocomposites from the amorphous state. Polym Eng Sci. 2011;51:1564–73.
48. Chen L, Dou Q. Influence of the combination of nucleating agent and plasticizer on the non-isothermal crystallization kinetics and activation energies of poly(lactic acid). J Therm Anal Calorim. 2020;139:1069–90.
49. dos Santos Silva ID, Schäfer H, Jaques NG, et al. An investigation of PLA/Babassu cold crystallization kinetics. J Therm Anal Calorim. 2020;141:1389–97.
50. Ries A, Canedo EL, Souto CR, Wellen RMR. Non-isothermal cold crystallization kinetics of poly(3-hydoxybutyrate) filled with zinc oxide. Thermochim Acta. 2016;637:74–81.
51. Li C, Dou Q, Bai Z, Lu Q. Non-isothermal crystallization behaviors and spherulitic morphology of poly(lactic acid) nucleated by a novel nucleating agent. J Therm Anal Calorim. 2015;122:407–17.
52. Di Lorenzo ML, Androsch R. Influence of α′-/α-crystal polymorphism on properties of poly(L-lactic acid). Polym Int. 2019;68:320–40.
53. Aliotta L, Cinelli P, Coltelli MB, Righetti MC, Gazzano M, Lazzeri A. Effect of nucleating agents on crystallinity and properties of poly (lactic acid) (PLA). Eur Polym J. 2017;93:822–32.
54. Chen X, Kalish J, Hsu SL. Structure evolution of α′-phase poly(lactic acid). J Polym Sci Part B Polym Phys. 2011;49:1446–54.
55. Běhálek L, Borůvka M, Brdlík P, Habr J, Lenfeld P, Kroisová D, et al. Thermal properties and non-isothermal crystallization kinetics of biocomposites based on poly(lactic acid), rice husks and cellulose fibres. J Therm Anal Calorim. 2020. https://doi.org/10.1007/s10973-020-09894-3.
56. Katiyar V. Bio-based plastics for food packaging applications. Shawbury: Smithers Pira; 2017.